Terahertz imaging with compressed sensing and phase retrieval

Wai Lam Chan,* Matthew L. Moravec, Richard G. Baraniuk, and Daniel M. Mittleman

Department of Electrical and Computer Engineering, Rice University, 6100 Main Street, Houston, Texas 77005, USA
**Corresponding author: wailam@rice.edu*

Received January 28, 2008; accepted March 5, 2008;
posted March 27, 2008 (Doc. ID 92168); published April 28, 2008

We describe a novel, high-speed pulsed terahertz (THz) Fourier imaging system based on compressed sensing (CS), a new signal processing theory, which allows image reconstruction with fewer samples than traditionally required. Using CS, we successfully reconstruct a 64×64 image of an object with pixel size 1.4 mm using a randomly chosen subset of the 4096 pixels, which defines the image in the Fourier plane, and observe improved reconstruction quality when we apply phase correction. For our chosen image, only about 12% of the pixels are required for reassembling the image. In combination with phase retrieval, our system has the capability to reconstruct images with only a small subset of Fourier *amplitude* measurements and thus has potential application in THz imaging with cw sources.

OCIS codes: 110.6795, 320.7100.

With applications to aerospace, homeland security, medical imaging, and quality control of packaged goods, time-domain terahertz (THz) imaging systems have proven valuable in numerous fields. However, these systems are generally limited by slow image acquisition rate [1]. In the fastest example of raster-scan THz imaging reported to date, a 400×400 pixel image takes as long as 6 min to acquire [2]. Recent developments using more sophisticated image processing approaches, such as the radon transform [3,4] and interferometric imaging [5], have shown preliminary successes but also face similar limitations in speed, resolution, and/or hardware requirements.

Meanwhile a newly developed theory in signal processing called compressed sensing (CS) has emerged. CS enables reconstruction of an image using many fewer measurements than are traditionally required [6,7]. This CS theory assumes that most real-world objects have a sparse representation in terms of some basis, meaning that most energy of an image can be compacted into just a few essential coefficients in some transform domain [6]. For image reconstruction, CS searches for the sparsest solution in the solution space based on the measurements via an optimization procedure. Major applications of CS to imaging have included tomography [7]; a single-pixel camera [8], which uses a single-pixel detector instead of a photodetector array for imaging in visible light; and hyperspectral imaging [9]. In each of these examples, the CS theory has inspired new imaging system designs, which feature simpler hardware and/or better imaging efficiency.

In this paper we describe the first example of CS applied to THz imaging. We demonstrate successful reconstruction of a target's image with a randomly chosen subset of the samples from the Fourier plane. We also combine CS with traditional phase retrieval (PR) algorithms [10] for image reconstruction with only a random subset of the Fourier amplitude image. Incorporation of CS into THz imaging system designs can significantly reduce the image acquisition time, since fewer measurements are required.

Our imaging system consists of a pulsed THz transmitter and receiver, both based on photoconductive antennas, and two lenses, one of which approximately collimates the THz beam while the other focuses the beam (see Fig. 1). The object mask, placed in between the two lenses, scatters the THz waves. The focusing lens forms the Fourier transform of the object mask at its focal plane. The receiver, mounted on a translation stage, performs a raster scan in the focal plane, over an area of 64×64 mm, at 1 mm intervals. We place a circular aperture (1 mm in diameter) in front of the receiver antenna so that it only samples a small area of the Fourier pattern, rather than relying on the ~6 mm receiver aperture [11]. The object mask is made of opaque copper tape on a transparent plastic plate. In our experiments, our object mask has an R-shaped hole, 34 mm height and 31 mm width.

At each detector position, an entire time-domain THz waveform is measured. We compute the power spectrum of each waveform and select the spectral amplitude and phase at a particular wavelength ($\lambda = 1.5$ mm) to obtain a (complex) pixel value. In this way, we assemble a 64×64 Fourier image. Direct 2D

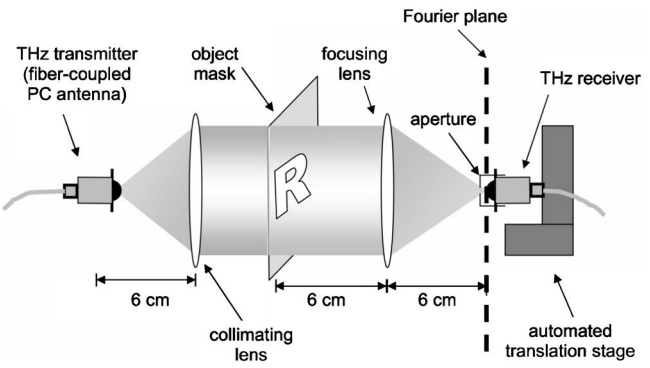

Fig. 1. THz Fourier imaging setup. An approximately collimated beam from the THz transmitter illuminates an object mask, placed one focal length away from the focusing lens. The THz receiver raster scans and samples the Fourier transform of the object on the focal plane.

0146-9592/08/090974-3/$15.00

Fourier inversion of this image reconstructs the object mask as shown in Fig. 2(a). The pixel size is given by $\Delta x = \lambda f / X$, where X is the length in one dimension of the raster-scan area (64 mm) and f is the focal length of the focusing lens (60 mm). Thus we obtain a pixel size of $\Delta x = 1.406$ mm in both dimensions, at the chosen wavelength.

To estimate the resolution of the reconstructed image in Fig. 2(a), we select a 5×15 region containing the left "leg" of the "R." After averaging the five selected rows, the resulting trace can be approximated by the convolution of a rectangular function with a Gaussian function with unknown variance (σ^2). We measure the width of the left leg of the R, i.e., the width of the rectangular function, to be 8 mm. We can then estimate σ^2 of the Gaussian function to fit the average trace. Our estimate for σ^2 is around 1 mm^2, equivalent to a full width at half-maximum (FWHM) of 2.354 mm or 1.68 pixels, which we define as the resolution of our reconstructed image. This 2D Fourier inversion technique requires measurements at all 4096 pixel locations and is therefore slow. Using CS, we can achieve good image reconstruction quality from only a small randomly chosen subset of these 4096 pixels, thus speeding up the imaging process.

Consider our object mask a length-N signal x of dimension indexed as $x(n)$, $n \in \{1, 2, \ldots, N\}$. In this case, x is a 2D image with pixels ordered in a $N \times 1$ vector, where $N = 4096$. We can view the Fourier measurements as projections, $y(m) = \langle x, \phi_m^T \rangle$, of the signal x onto a set of Fourier basis functions $\{\phi_m\}$, $m \in \{1, 2, \ldots, M\}$, where ϕ_m^T denotes the transpose of ϕ_m and $\langle \cdot, \cdot \rangle$ denotes the inner product. For direct 2D Fourier inversion, we acquire $M = N = 4096$ measurements for image reconstruction. However, in CS, we use only a much smaller number of measurements than the number of pixels in the image, i.e., $M < N$. In matrix notation, we measure $y = \Phi x$, where y is an $M \times 1$ column vector of measurements and the measurement matrix Φ is $M \times N$. Despite using fewer measurements, we can still reconstruct the object perfectly, assuming its sparsity, through an optimization procedure [6].

Many optimization algorithms exist to solve this inverse imaging problem. These algorithms aim to find the solution with the smallest $l1$ norm, i.e., to solve the minimization problem

$$\arg\min \|x\|_1 \quad \text{subject to constraint } y = \Phi x, \qquad (1)$$

where $\|\cdot\|_1$ denotes the $l1$-norm [6]. Sometimes, when the original image x is sparse in another reconstruction basis Ψ (such as wavelets), we substitute $x = \Psi \theta$ in the constraint in Eq. (1) and solve for the minimum $l1$-norm of θ instead. We obtain the reconstruction result in Fig. 2(b) using only 500 measurements out of the total 4096 measurements through the SPGL1 algorithm described by van den Berg and Friedlander [12]. Using CS, we reduce the number of measurements required for image formation by more than a factor of 8.

We desire to further improve the reconstruction result by removing the background profile of the phase, which is not due to the object but is inherent in the spherical wavefront curvature of the Gaussian beam illumination of the object [see Fig. 2(d)]. As a result, the phase in the Fourier plane is distorted by the superposition of a spherically varying background. We first remove the object mask in our setup and obtain a 64×64 image of the background phase of the beam through 2D Fourier inversion. These phase values at each pixel form the diagonal entries of a matrix P. Similar to the modification suggested by Lustig *et al.*

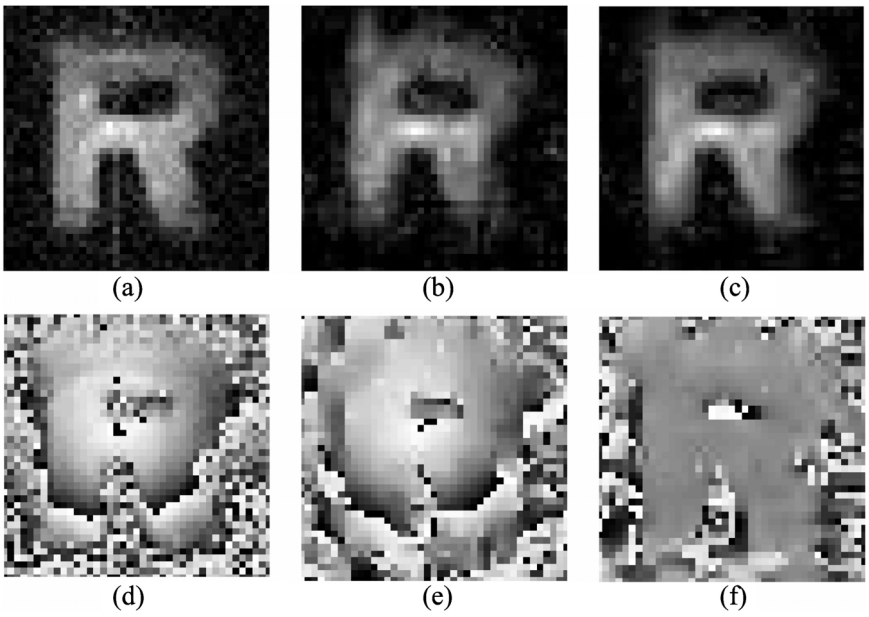

Fig. 2. Compressed sensing imaging results. (a) Magnitude of image reconstructed by inverse Fourier transform using the full dataset (4096 uniformly sampled measurements) and (d) its phase. Note the phase distortion inherent in the THz beam in (d). Compressed sensing reconstruction result using 500 measurements (12%) from the full dataset: (b) magnitude and (e) phase. Compressed sensing with phase correction improves image quality and eliminates phase distortion [see (c) and (f)]. All figures show a zoom-in view on a 40×40 grid centered on the object.

[13], we insert this diagonal matrix P after Φ in Eq. (1) and then solve the phase-corrected optimization problem for image reconstruction. This phase-correction procedure not only removes the spherically varying phase profile in the reconstruction [compare Fig. 2(f) to Figs. 2(d) and 2(e)] but also improves the quality of the reconstruction [compare Fig. 2(c) to Fig. 2(b)]. Using the same procedure as for Fig. 2(a), we obtain a resolution of 4.19 and 3.35 pixels for Figs. 2(b) and 2(c), respectively. Since an object with a constant phase profile has a more sparse representation in wavelet basis than one with a spatially varying phase profile, CS reconstruction using phase correction yields superior performance for a given number of measurements.

If we move the object mask in Fig. 1 away from the object plane, the acquired Fourier data will have the correct Fourier magnitude but a distorted phase. We can no longer use the phase data for image reconstruction. However, we can still reconstruct an image by combining CS with the well-known technique of PR [10]. Moravec *et al.* recently developed a PR minimization algorithm, called compressive phase retrieval (CPR), which uses the full Fourier amplitude dataset [14]. The same paper also describes a compressive sensing phase retrieval (CSPR) algorithm, which enables reconstruction with a subset of the Fourier amplitude samples. It is particularly challenging for PR to reconstruct complex-valued images of objects with a nonuniform phase profile. Therefore, we modify the original Fourier dataset such that, when applying the CPR and CSPR algorithms, we assume that the illuminating beam is a perfect plane wave. We first obtain the inverse Fourier image of the object (magnitudes and phases) as in Figs. 2(a) and 2(d) from the 4096 measurements. Then, we keep the magnitude of this spatial image unaltered but remove its phase using the background phase profile of the beam. The magnitude of the Fourier transform of this phase-corrected spatial image is the input to our CPR and CSPR algorithms. Figures 3(a) and 3(b) show the reconstruction results from CPR with the full dataset and from CSPR with 1500 measurements, respectively.

Our CSPR reconstruction results demonstrate the applicability of our imaging scheme not only to pulsed THz imaging systems but also to cw systems, in which phase information is typically not available.

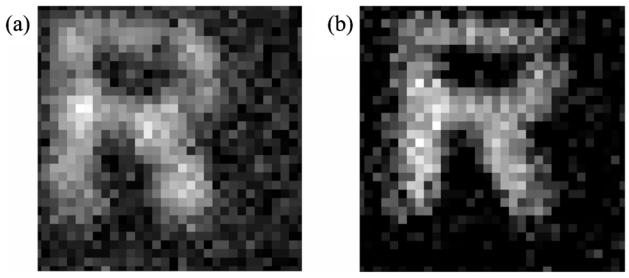

Fig. 3. Image reconstruction results using (a) CPR with the full dataset (4096 magnitude measurements) and (b) CSPR with a subset of 1500 measurements from the dataset used in (a).

The latest research on THz cw imaging requires high-power sources (>10 mW), such as quantum-cascade lasers operating at low temperature (~30 K), because the focal-plane microbolometer array used for imaging has low sensitivity at THz frequencies [15]. In contrast, our Fourier imaging technique with CSPR can use a single-pixel THz detector with much higher sensitivity to enable imaging with a low-power cw source.

In conclusion, we have shown the CS reconstruction of THz images using significantly fewer measurements than a conventional raster-scan imaging technique. Our resulting THz Fourier imaging system successfully recovers the test object with pixel size 1.4 mm, using only about 12% of the 4096 pixels. We have also demonstrated an improvement of CS reconstruction quality using phase correction and successful image reconstruction with only the Fourier amplitude using CSPR. Our transmission setup in this Letter could be useful for quality control applications, such as detection of point impurities in manufactured products, because Fourier-domain measurements are particularly sensitive to sharp pointlike features. Additional work is required to efficiently combine acquired data across frequencies to enhance both the CS and the CSPR reconstruction results.

This research has been supported in part by the National Science Foundation and the National Aeronautics and Space Administration.

References

1. W. L. Chan, J. Deibel, and D. M. Mittleman, Rep. Prog. Phys. **70**, 1325 (2007).
2. D. Zimdars, Proc. SPIE **5692**, 255 (2005).
3. S. Wang and X.-C. Zhang, J. Phys. D: Appl. Phys. **37**, R1 (2004).
4. J. Pearce, H. Choi, and D. M. Mittleman, Opt. Lett. **30**, 1653 (2005).
5. A. Bandyopadhyay, A. Stepanov, B. Schulkin, M. D. Federici, A. Sengupta, D. Gary, J. F. Federici, R. Barat, Z.-H. Michalopoulou, and D. Zimdars, J. Opt. Soc. Am. A **23**, 1168 (2006).
6. D. Donoho, IEEE Trans. Inf. Theory **52**, 1289 (2006).
7. E. Candes, J. Romberg, and T. Tao, IEEE Trans. Inf. Theory **52**, 489 (2006).
8. D. Takhar, J. Laska, M. Wakin, M. Duarte, D. Baron, S. Sarvotham, K. Kelly, and R. Baraniuk, Proc. SPIE **6065**, 606509 (2006).
9. M. E. Gehm, R. John, D. J. Brady, R. M. Willett, and T. J. Schulz, Opt. Express **15**, 14013 (2007).
10. J. R. Fienup, Opt. Lett. **3**, 27 (1978).
11. M. T. Reiten, S. A. Harmon, and R. A. Cheville, J. Opt. Soc. Am. B **20**, 2215 (2003).
12. E. van den Berg and M. P. Friedlander, SPGL1: a solver for large-scale sparse reconstruction, http://www.cs.ubc.ca/labs/scl/spgl1 (2007).
13. M. Lustig, D. Donoho, and J. M. Pauly, Magn. Reson. Med. **58**, 1182 (2007).
14. M. L. Moravec, J. K. Romberg, and R. G. Baraniuk, Proc. SPIE **6701**, 670120 (2007).
15. A. W. M. Lee, Q. Qin, S. Kumar, B. S. Williams, Q. Hu, and J. L. Reno, Appl. Phys. Lett. **89**, 141125 (2006).